INL/CON-21-65062-Revision-0

Coupling coarse mesh CFD with fine mesh CFD for modeling for Molten Salt Reactors in the Virtual Test Bed VTB

May 2022

Mauricio Eduardo Tano Retamales, Abdalla Abou Jaoude, Ramiro Freile, Jun Fang, Dillon Shaver

Changing the World's Energy Future

INL is a U.S. Department of Energy National Laboratory operated by Battelle Energy Alliance, LLC

DISCLAIMER

This information was prepared as an account of work sponsored by an agency of the U.S. Government. Neither the U.S. Government nor any agency thereof, nor any of their employees, makes any warranty, expressed or implied, or assumes any legal liability or responsibility for the accuracy, completeness, or usefulness, of any information, apparatus, product, or process disclosed, or represents that its use would not infringe privately owned rights. References herein to any specific commercial product, process, or service by trade name, trade mark, manufacturer, or otherwise, does not necessarily constitute or imply its endorsement, recommendation, or favoring by the U.S. Government or any agency thereof. The views and opinions of authors expressed herein do not necessarily state or reflect those of the U.S. Government or any agency thereof.

INL/CON-21-65062-Revision-0

Coupling coarse mesh CFD with fine mesh CFD for modeling for Molten Salt Reactors in the Virtual Test Bed VTB

Mauricio Eduardo Tano Retamales, Abdalla Abou Jaoude, Ramiro Freile, Jun Fang, Dillon Shaver

May 2022

Idaho National Laboratory
Idaho Falls, Idaho 83415

http://www.inl.gov

Prepared for the
U.S. Department of Energy
Under DOE Idaho Operations Office
Contract DE-AC07-05ID14517

Coupling Coarse-Mesh CFD with Fine-Mesh CFD for Modeling for Molten-Salt Reactors in the Virtual Test Bed (VTB)

Tano M[1,2*], Freile R[2], Fang J[3], Abou-Jaoude A[1], Sahver D[3]

[1] Idaho National Laboratory
P.O. Box 1625, Idaho Falls, ID 83415

[2]Nuclear Engineering Department, Texas A&M University
423 Spence St, College Station, TX 77843

[3]Argonne National Laboratory
9700 S Cass Ave, Lemont, IL 60439

mauricio.tanoretamales@inl.gov, freiler@tamu.edu, fangj@inl.gov,
abdalla.aboujaoude@inl.gov, dshaver@anl.gov

[leave space for DOI, which will be inserted by ANS]

ABSTRACT

The Nuclear Energy Advanced Modeling and Simulation (NEAMS) program aims at developing a simulation tool kit to accelerate the development and deployment of nuclear power technologies. NEAMS multiphysics tools have been designed to provide numerical simulation support for the design and licensing of GEN IV reactors. Pronghorn is NEAMS's coarse-mesh computational fluid dynamics (CFD) tool, which is designed to run 3D core transients in GEN IV reactors at a reduced computational cost. To increase their accuracy, coarse-mesh CFD simulations require calibrated closure coefficients. One way of computing these coefficients is via the Nek5000, NEAMS's high-fidelity CFD tool. This article discusses our current research lines in informing Pronghorn closure coefficients via Nek5000 to enable multiphysics simulations of the core cavity of the molten-salt fast reactor. We present an application in which Pronghorn mixing length turbulent viscosity has been calibrated from Nek5000 simulations. The resulting Pronghorn thermal-hydraulics model is then coupled to Griffin, the NEAMS neutron transport solver, to solve for the steady-state configuration of the molten-salt fast reactor.

KEYWORDS: CFD, intermediate-fidelity, high-fidelity, coupling

1. INTRODUCTION

GEN IV reactors require a suite of multiphysics tools for design, optimization, and licensing. The NEAMS packages [1] supports this need among Department of Energy labs. NEAMS tools have previously been used for the design and evaluation of molten-salt [2], high-temperature [3,4] and liquid-metal [5] reactors, between others. As part of the Virtual Test Bed (VTB) project*—a collaboration between NEAMS and the National Reactor Innovation Center

(NRIC)—a host of challenge multiphysics problems are being developed to set up a foundational analysis for these advanced reactors [5]. One of the current challenges in NEAMS is coupling the different standalone modules to provide an integrated multiphysics, multi-fidelity code suite. This would involve different aspects of reactor physics, including neutronics, thermal hydraulics, structural thermomechanics, etc. This is of particular importance in the tightly coupled behavior of molten-salt reactors (MSR). While neutron transport codes have well established reduced-order models (e.g., diffusion approximation, super-homogenization) and finite element thermomechanics calculations are relatively inexpensive, multidimensional thermal-hydraulic options are limited. As a result, this article will focus on leveraging Nek5000 [6], a high-fidelity computational fluid dynamics (CFD) tool, to inform Pronghorn [7], a coarse-mesh thermal-hydraulic (TH) tool. Ultimately, the end goal is to leverage these Nek-informed Pronghorn models and couple them to the Griffin [8] neutronic solver as well as MOOSE-based models.

As previously stated, a key component of MSR multiphysics simulation is neutronics. Griffin is specially designed to support multiphysics applications and to natively couple to any Multiphysics Object-Oriented Simulation Environment (MOOSE) application, including Pronghorn. It is a time-dependent reactor physics code built using the MOOSE framework with weak form formulations for diffusion, PN, and first- and second-order SN transport with a variety of equivalence techniques with acceleration. The code stems from the merger of two other Department of Energy codes: Rattlesnake [9] and Proteus [10].

Pronghorn is part of the ongoing effort within the MOOSE ecosystem [11] to develop fast core simulators using an intermediate-fidelity approach. It adopts a coarse-mesh porous media formulation that avoids solving for lower-length scale phenomena, such as boundary layers or turbulent mixing, relying instead on closure correlations. Closure correlations can be either inherent to the physical formulation of the fluid flow equations in Pronghorn (e.g., turbulent eddy viscosity or turbulent eddy diffusivity) or to the coarse-mesh discretization approach adopted in this tool (e.g., solid-fluid friction factors or heat exchange coefficients). This article will focus on improving turbulence modeling in Pronghorn, for which either experiments or higher-fidelity tools are needed to inform closure correlations.

Nek5000 is NEAMS's high-fidelity CFD tool based on the spectral element method (SEM). SEM combines the accuracy of spectral methods with the domain flexibility of the finite element method. It is highly parallel and has been previously applied to a wide range of problems to gain unprecedented insight into the complex flow physics in nuclear reactor systems. A considerable amount of literature has been published on various Nek5000 applications for nuclear reactor designs, ranging from conventional light-water reactors to advanced reactors, such as MSRs, sodium-cooled fast reactor, etc. [12–15]. Nek5000 offers accurate fluid simulations at multiple resolution requirements, from the first-principle-based direct numerical simulation to the efficient Reynolds-averaged Navier-Stokes (RANS) modeling [16–18]. Thus, Nek5000 is selected herein to generate the high-fidelity CFD reference data to inform the turbulence modeling in Pronghorn.

Broadly, the high-to-intermediate-fidelity coupling strategies analyzed can be divided into intrusive or non-intrusive. In the intrusive method, the set of governing equations for the high-fidelity model are projected into a reduced system, which is then expanded to compute the space-

time-dependent closure variables for the intermediate-fidelity one. Non-intrusive methods exploit the data produced by high-fidelity simulations to develop a set of closure correlations for the intermediate-fidelity ones. Closure correlations will depend on the structural form assumed for the intermediate-fidelity model and the regression method used to map high-fidelity data into this structural form.

This article will focus in utilizing Nek5000 high-fidelity data to improve turbulence modeling in Pronghorn. We take this as a representative example of our current line of research in coupling multi-fidelity simulations within the NEAMS framework, which are also discussed in the current paper.

2. MODELING FRAMEWORK

2.1. Basic Modeling Equations

For the high-fidelity model, an incompressible Navier-Stokes formulation is considered in the current study, of which the governing equations solved by Nek5000 are given by

$$\rho\left[\frac{\partial u_i^{hf}}{\partial t}+\frac{\partial}{\partial x_j}\left(u_i^{hf}u_j^{hf}\right)\right]=-\frac{\partial p^{hf}}{\partial x_i}+\frac{\partial}{\partial x_j}\left[\left(\mu+\mu_t^{hf}\right)\left(\frac{\partial u_i^{hf}}{\partial x_j}+\frac{\partial u_j^{hf}}{\partial x_i}\right)\right]+f_{firc,i}^{hf}+F_i^{hf} \quad (1)$$

$$\frac{\partial u_i^{hf}}{\partial x_i}=0 \quad (2)$$

where the super-script hf denotes the high-fidelity Reynolds-averaged variable, u_i^{hf} is velocity in the i direction, p^{hf} is the pressure, ρ is the fluid density, F_i^{hf} denotes the body force term in the i^{th} direction, μ and μ_t^{hf} are the kinematic and high-fidelity turbulent viscosities, respectively, and $f_{firc,i}^{hf}$ is a volumetric factor. μ_t^{hf} can be calculated from the turbulent scalars in the k - τ model[5] as follows

$$\rho\frac{\partial k^{hf}}{\partial t}+\rho\frac{\partial}{\partial x_j}\left(k^{hf}u_j^{hf}\right)=\frac{\partial}{\partial x_k}\left[\left(\mu+\frac{\mu_t^{hf}}{\sigma_k}\right)\frac{\partial k^{hf}}{\partial x_k}\right]+P^{hf}-\rho\beta^*\frac{k^{hf}}{\tau^{hf}} \quad (3)$$

$$\frac{\partial\left(\rho\tau^{hf}\right)}{\partial t}+\frac{\partial}{\partial x_j}\left(\rho\tau^{hf}u_j^{hf}\right)=\nabla\cdot\left[\left(\mu+\frac{\mu_t}{\sigma_\tau}\right)\nabla\tau^{hf}\right]-\gamma\frac{\tau^{hf}}{k^{hf}}P+\rho\beta-2\frac{\mu}{\tau^{hf}}\left(\nabla\tau^{hf}\cdot\nabla\tau^{hf}\right) \quad (4)$$

$$\mu_t^{hf}=\rho k^{hf}\tau^{hf} \quad (5)$$

where $P=\left(\mu+\mu_t^{hf}\right)\left(\frac{\partial u_i^{hf}}{\partial x_j}+\frac{\partial u_j^{hf}}{\partial x_i}\right)\frac{\partial u_i^{hf}}{\partial x_j}$ is the turbulent kinetic energy production and β^*, β, and γ are scaling functions. We refer the reader to [16] for details on the closure terms of this model.

On the other hand, we also assume an incompressible flow model in Pronghorn, but with a coarser mesh and a different turbulence closure model. This model reads as follows:

$$\rho\left[\frac{\partial u_i^{if}}{\partial t}+\frac{\partial}{\partial x_j}\left(u_i^{if}u_j^{if}\right)\right]=-\frac{\partial p^{if}}{\partial x_i}+\frac{\partial}{\partial x_j}\left[\left(\mu+\mu_t^{if}\right)\left(\frac{\partial u_i^{if}}{\partial x_j}+\frac{\partial u_j^{if}}{\partial x_i}\right)\right]+f_{firc,i}^{if}+F_i^{if} \tag{6}$$

$$\frac{\partial u_i^{if}}{\partial x_i}=0 \tag{7}$$

$$\mu_t^{if}=\mathcal{F}_t^{if}\left(u^{if},p^{if},\frac{\partial u^{if}}{\partial x_j},\frac{\partial p^{if}}{\partial x_i},t,p_d,p_c\right) \tag{8}$$

where the super-script if represents the intermediate-fidelity variable and $\mathcal{F}_t^{if}$ represents a generic turbulence closure function for the intermediate-fidelity model. This closure is a function of the intermediate-fidelity velocity u^{if} and pressure p^{if}, its space gradients, time t, and a set of parameters p_d, describing the geometry of the problem (e.g., density, viscosity, or the distance to the walls, etc.), and p_c are a set of colure parameters or fields (e.g., closure constants, damping functions, etc.). The high-to-low-fidelity turbulence mapping consists of finding a model for $\mathcal{F}_t^{if}$ and of calibrating it using high-fidelity data.

2.2. Intrusive High-to-Intermediate-Fidelity Mapping

Numerically, once discretized, the high-fidelity model reads as follows:

$$\boldsymbol{A}\left(\boldsymbol{u}^{hf,(n-1)}\right)\boldsymbol{u}^{hf}=-\boldsymbol{B}^T\boldsymbol{p}^{hf}+\boldsymbol{f}_{firc,i}^{hf}+\boldsymbol{F}_i^{hf} \tag{9}$$

$$\boldsymbol{B}\boldsymbol{u}^{hf}=0 \tag{10}$$

$$\boldsymbol{C}\left(\boldsymbol{u}^{hf},\boldsymbol{\tau}^{hf}\right)\boldsymbol{k}^{hf}=\boldsymbol{P}^{hf} \tag{11}$$

$$\boldsymbol{D}\left(\boldsymbol{u}^{hf},\boldsymbol{k}^{hf},\boldsymbol{\tau}^{hf,(n-1)}\right)\boldsymbol{\tau}^{hf}=\rho\boldsymbol{\beta} \tag{12}$$

$$\boldsymbol{\mu}_t^{hf}=\rho\boldsymbol{k}^{hf}\boldsymbol{\tau}^{hf} \tag{13}$$

After exercising the model on a set of samples of $\{\rho\}=\{\rho_1,\dots,\rho_s\}$ and $\{\mu\}=\{\mu_1,\dots,\mu_s\}$, uniquely defining a set of Reynolds numbers, one obtains a set of solutions for the velocity ($\{\boldsymbol{u}^{hf}\}=\{\boldsymbol{u}^{hf}(\{\rho\},\{\mu\})\}\in\mathbb{R}^{3\,n_{dof}\times s}$), pressure ($\{\boldsymbol{p}^{hf}\}=\{\boldsymbol{p}^{hf}(\{\rho\},\{\mu\})\}\in\mathbb{R}^{n_{dof}\times s}$), turbulent kinetic energy ($\{\boldsymbol{k}^{hf}\}=\{\boldsymbol{k}^{hf}(\{\rho\},\{\mu\})\}\in\mathbb{R}^{n_{dof}\times s}$), the inverse of its specific dissipation rate ($\{\boldsymbol{\tau}^{hf}\}=\{\boldsymbol{\tau}^{hf}(\{\rho\},\{\mu\})\}\in\mathbb{R}^{n_{dof}\times s}$), and the turbulent viscosity ($\{\boldsymbol{\mu}^{hf}\}=\{\boldsymbol{\mu}^{hf}(\{\rho\},\{\mu\})\}\in\mathbb{R}^{n_{dof}\times s}$). Then, data compression methods, such as proper orthogonal decomposition, can be used to extract a set of $r(<s\ll n_{dof})$ principal modes for the velocity ($\boldsymbol{U}_{\boldsymbol{u}}^{\boldsymbol{hf}}\in\mathbb{R}^{3n_{dof}\times r}$), pressure ($\boldsymbol{U}_{\boldsymbol{p}}^{\boldsymbol{hf}}\in\mathbb{R}^{n_{dof}\times r}$), turbulent kinetic energy ($\boldsymbol{U}_{\boldsymbol{k}}^{\boldsymbol{hf}}\in\mathbb{R}^{n_{dof}\times r}$), the inverse of its specific turbulent dissipation ($\boldsymbol{U}_{\boldsymbol{\tau}}^{\boldsymbol{hf}}\in\mathbb{R}^{n_{dof}\times r}$), and the turbulent viscosity ($\boldsymbol{U}_{\boldsymbol{\mu}}^{\boldsymbol{hf}}\in\mathbb{R}^{n_{dof}\times r}$). These modes can then be used to propose a reduced representation of the previous fields as $\boldsymbol{\phi}^{hf}=\boldsymbol{U}_{\phi}^{hf}\boldsymbol{c}_{\phi}^{hf}$, where ϕ^{hf} generically represents the previous high-fidelity fields and $\boldsymbol{c}_{\phi}^{hf}\in\mathbb{R}^r$ are the projection coefficients of the reduced system over the high-fidelity fields. Introducing the reduced representation of the high-fidelity fields and introducing a Galerkin projection on these modes, we end up with a reduced representation of the high-fidelity system, which reads as follows:

$$\boldsymbol{U_u^{hf}}^T \boldsymbol{A}\left(\boldsymbol{U_u^{hf}}\boldsymbol{c_u}^{hf,(n-1)}\right)\boldsymbol{U_u^{hf}}\boldsymbol{c_u}^{hf,(n-1)} = -\boldsymbol{U_u^{hf}}^T\boldsymbol{B}^T\boldsymbol{U_c^{hf}}\boldsymbol{c_p}^{hf} + \boldsymbol{U_u^{hf}}^T\boldsymbol{f}_{irc,i}^{hf} + \boldsymbol{U_u^{hf}}^T\boldsymbol{F}_i^{hf} \in \mathbb{R}^{3r} \quad (14)$$

$$\boldsymbol{U_u^{hf}}^T\boldsymbol{B}\boldsymbol{U_c^{hf}}\boldsymbol{c_u}^{hf} = 0 \in \mathbb{R}^r \quad (15)$$

$$\boldsymbol{U_k^{hf}}^T\boldsymbol{C}\left(\boldsymbol{U_u^{hf}}\boldsymbol{c_u}^{hf}, \boldsymbol{U_\tau^{hf}}\boldsymbol{c_\tau}^{hf}\right)\boldsymbol{U_k^{hf}}\boldsymbol{c_k}^{hf} = \boldsymbol{U_k^{hf}}^T\boldsymbol{P}^{hf} \in \mathbb{R}^r \quad (16)$$

$$\boldsymbol{U_\tau^{hf}}^T\boldsymbol{D}\left(\boldsymbol{U_u^{hf}}\boldsymbol{u}^{hf}, \boldsymbol{U_k^{hf}}\boldsymbol{k}^{hf}, \boldsymbol{U_\tau^{hf}}\boldsymbol{\tau}^{hf,(n-1)}\right)\boldsymbol{U_\tau^{hf}}\boldsymbol{c_\tau}^{hf} = \boldsymbol{U_\tau^{hf}}^T\rho\boldsymbol{\beta} \in \mathbb{R}^r \quad (17)$$

$$\boldsymbol{c}_{\boldsymbol{\mu}_t}^{hf} = \boldsymbol{U}_{\boldsymbol{\mu}_t}^{hf^T}\left(\rho\boldsymbol{U_k^{hf}}\boldsymbol{c}_k^{hf}\boldsymbol{U_\tau^{hf}}\boldsymbol{\tau}^{hf}\right) \in \mathbb{R}^r \quad (18)$$

Note that the multiplications of the form $\boldsymbol{U^T U}$ can be pre-computed before exercising the model, leading to a computationally inexpensive solution that scales with order r. One could stop at this point and directly use this reduced system to compute the thermal-hydraulics fields. Nonetheless, as we previously showed in [19], the numerical stability issues on this system could yield large errors. Therefore, we are currently researching an alternative approach, which consists of introducing the resolved turbulent field into a coarse-mesh turbulence model.

The intermediate-fidelity model can also be exercised for the samples of the parameters $\{\rho\}, \{\mu\}$, and dimensionality reduction can be performed on the turbulent viscosity snapshots, leading to a reduced representation as follows $\boldsymbol{\mu_t^{if}} = \boldsymbol{U}_{\boldsymbol{\mu_t}}^{if}\boldsymbol{c}_{\boldsymbol{\mu}_t}^{if}$. Now, restricting the reduced representation of the turbulent viscosity to r modes, we can impose the constraint $\boldsymbol{c}_{\boldsymbol{\mu}_t}^{if} = \boldsymbol{c}_{\boldsymbol{\mu}_t}^{hf}$, leading to a high-fidelity informed intermediate-fidelity turbulent viscosity as follows:

$$\boldsymbol{\mu_t^{if}} = \left(\boldsymbol{U}_{\boldsymbol{\mu_t}}^{if}\boldsymbol{U}_{\boldsymbol{\mu_t}}^{hf^T}\right)\left(\rho\boldsymbol{U_k^{hf}}\boldsymbol{c}_k^{hf}\boldsymbol{U_\tau^{hf}}\boldsymbol{\tau}^{hf}\right) \in \mathbb{R}^r \quad (19)$$

Results of this approach are not provided in the present version of this article but will be provided at the revision stage. One of the issues of this intrusive approach is that access to the numerical discretization of the high-fidelity system is required to develop the reduced system in Equations (14)–(18). Non-intrusive approaches do not present this constraint.

2.3. Non-Intrusive High-to-Intermediate-Fidelity Mapping

The non-intrusive mapping is methodologically simpler than the intrusive one, but it imposes higher constraints on the projected correlations. Similar to the intrusive approach, the procedure starts with the development of full order on samples of density $\{\rho\}$ and dynamic viscosity $\{\mu\}$. This yields a set of fields for the high-fidelity turbulent viscosity $\{\boldsymbol{\mu}^{hf}\}$, velocity $\{\boldsymbol{u}^{hf}\}$, and pressure $\{\boldsymbol{p}^{hf}\}$. This set of results can be used to propose a functional spatial representation for dynamic viscosity as follows:

$$\{\boldsymbol{\mu}^{hf}\}(\boldsymbol{x}) = \mathcal{F}_t^{hf}\left(\{\boldsymbol{u}^{hf}\}(\boldsymbol{x}), \{\boldsymbol{p}^{hf}\}(\boldsymbol{x}), \frac{\partial\{\boldsymbol{u}^{hf}\}}{\partial x_j}(\boldsymbol{x}), \frac{\partial\{\boldsymbol{p}^{hf}\}}{\partial x_i}(\boldsymbol{x}), t, p_d\right) \quad (20)$$

Different regression approaches can be used for computing the high-fidelity mapping function, such as linear regression, radial-basis function regression, or deep neural networks. We refer the reader to [20] for details on how regression methods perform in reconstructing the turbulent

viscosity field. Once calibrated, the regressor $\mathcal{F}_t^{hf}$ can be conceived as a functor that takes the current velocity, pressure, gradients, time, and parametric descriptors for a cell and outputs the turbulent viscosity. Therefore, for the intermediate-fidelity method, one can make the analogy $\mathcal{F}_t^{if} \approx \mathcal{F}_t^{hf}$, which allows us to obtain a turbulent viscosity mapping method in the intermediate-fidelity model that is defined by the high-fidelity one.

Note, however, that in this formulation, the turbulent viscosity found may be inconsistent with the realizable turbulent states, as there are no physical restrictions on the mapping operator $\mathcal{F}_t^{hf}$. Hence, we examined a different approach, which consists of using the high-fidelity mapping to compute specific closure fields p_c of the intermediate-fidelity viscosity model instead of the complete turbulent viscosity field. In this approach, samples of the intermediate-fidelity closure fields are collected while running the high-fidelity simulations, and the regression model is trained for these closure parameters as follows:

$$\{\boldsymbol{p_d}^{hf}\}(\boldsymbol{x}) = \tilde{\mathcal{F}}_t^{hf}\left(\{\boldsymbol{u}^{hf}\}(\boldsymbol{x}), \{\boldsymbol{p}^{hf}\}(\boldsymbol{x}), \frac{\partial\{\boldsymbol{u}^{hf}\}}{\partial x_j}(\boldsymbol{x}), \frac{\partial\{\boldsymbol{p}^{hf}\}}{\partial x_i}(\boldsymbol{x}), t, p_d\right) \tag{21}$$

Next, the intermediate-fidelity turbulent viscosity is computed as follows:

$$\mu_t^{if} = \mathcal{F}_t^{if}\left(u^{if}, p^{if}, \frac{\partial u^{if}}{\partial x_j}, \frac{\partial p^{if}}{\partial x_i}, t, p_d, p_c = \tilde{\mathcal{F}}_t^{hf}\left(u^{if}, p^{if}, \frac{\partial u^{if}}{\partial x_j}, \frac{\partial p^{if}}{\partial x_i}, t, p_d\right)\right) \tag{22}$$

where the physical realizability of turbulent in the model is provided by the imposed structural function $\mathcal{F}_t^{if}$ and the high-fidelity information of this model is provided by the computation of the closure fields by $\tilde{\mathcal{F}}_t^{hf}$.

Further results on non-intrusive coupling will be presented in the following revisions of this article. However, as an example of this procedure, a non-intrusive high-to-intermediate-fidelity mapping, where the structural form of the intermediate-fidelity model is computed via a capped mixing length model, is presented in the following subsection.

2.4. Application of Non-Intrusive High-to-Intermediate-Fidelity Mapping via a Capped Mixing Length Model

A capped mixing length model is assumed as the structural form for the turbulent viscosity in the intermediate-fidelity model. This model reads as follows:

$$\mu_t^{if} = \rho\, \ell_m^{2,if} \left|2S_{ij}^{if} S_{ij}^{if}\right|, S_{ij}^{if} = \frac{1}{2}\left(\frac{\partial u_i^{if}}{\partial x_j} + \frac{\partial u_j^{if}}{\partial x_i}\right) \tag{23}$$

The capping is performed in the mixing length model, and it reads as follows:

$$\begin{aligned} \ell_m^{if} &= \kappa y_d \;\; if\; \kappa y_d < \kappa_0 \delta \\ \ell_m^{if} &= \kappa_0 \delta^{if} \;\; if\; \kappa y_d \geq \kappa_0 \delta \end{aligned} \tag{24}$$

where $\kappa = 0.41$ is the Von Karman constant, $\kappa_0 = 0.09$ is a contant in Escudier's model, y_d is the distance to the wall, and δ is the tunable variable with length units that represents the extension of the boundary layer.

Samples of the high-fidelity model at different densities $\{\rho\}$ and viscosities $\{\mu\}$ have been generated and the resulting steady-state turbulent viscosity $\{\boldsymbol{\mu}_t^{hf}\}(\boldsymbol{x})$, velocity $\{\boldsymbol{u}^{hf}\}(\boldsymbol{x})$, and pressure $\{\boldsymbol{p}^{hf}\}(\boldsymbol{x})$ fields have been computed. The samples of the velocity field can be differentiated in space to construct the share strain rate tensors samples $\{\boldsymbol{S}^{hf}\}(\boldsymbol{x}) = 0.5(\nabla\{\boldsymbol{u}^{hf}\}(\boldsymbol{x}) + \nabla\{\boldsymbol{u}^{hf}\}^T(\boldsymbol{x}))$. Using these tensors, we can compute the set of samples for the mixing length as follows:

$$\{\ell_m^{2,hf}\}(\boldsymbol{x}) = \frac{\{\boldsymbol{\mu}_t^{hf}\}(\boldsymbol{x})}{\rho|2\{\boldsymbol{S}^{hf}\}(\boldsymbol{x})\{\boldsymbol{S}^{hf}\}(\boldsymbol{x})|} \tag{25}$$

Similarly, once the mixing lengths are obtained, we can compute a set of effective capping constants for the mixing length model using the second expression in Equation (24) as follows:

$$\{\delta^{hf}\}(\boldsymbol{x}) = \frac{\{\ell_m^{2,hf}\}(\boldsymbol{x})}{\kappa_0} \;\; if \; \kappa y_d \geq \{\ell_m^{2,hf}\}(\boldsymbol{x}) \tag{26}$$

Next, noting the dependence of the problem on the sampled density, viscosity, and inlet velocity boundary condition, which uniquely define the Reynolds number, we propose a capping for the mixing length as $\delta^{hf} = \delta^{hf}(Re)$ and use exponential regression to calibrate the model. Finally, we make the analogy $\delta^{if} \approx \delta^{hf}$ and obtain a high-fidelity informed turbulence model for the intermediate-fidelity one.

3. RESULTS

3.1. Molten-Salt Fast Reactor Model

The VTB's MSR model, presented in Figure 1, is based on the 2D axisymmetric molten-salt fast reactor (MSFR) model created under the Euratom EVOL (Evaluation and Viability of Liquid Fuel Fast Reactor Systems) and ROSATOM MARS (Minor Actinides Recycling in Molten Salt) projects [8]. The model includes a core region, a pump, and a heat exchanger. Both the pump and the heat exchanger are modeled as homogenous regions, adding a volumetric force at the pump to produce the liquid fuel circulation and a Forchheimer type resistance at the heat exchanger of the form $f_{fric,i}^{if} = -C_q u_i^{if}|\boldsymbol{u}^{if}|$, where C_q is a constant that is tuned to achieve the desired circulation speed. An interior reflector shields the pump and heat exchanger from the high neutron flux in the core. The model also includes an outer reflector surrounding all of the components. The reactor has a fast neutron spectrum and 3 GW of thermal power. The composition of the fuel salt is 19.985% ThF4, 2.515% U233F4, and 77.5% LiF (by mole). The nominal inlet and outlet salt temperatures are $650°C$ and $750°C$, respectively. A nickel alloy is assumed for the inner and outer reflectors. Most parameters and material properties of the VTB MSFR are taken from. That reference specifies a block-style geometry with all 90-degree angles, but a geometry with curved surfaces that more closely matches "Geometry II" from is used here. We refer the reader to the VTB website for more details of this model.

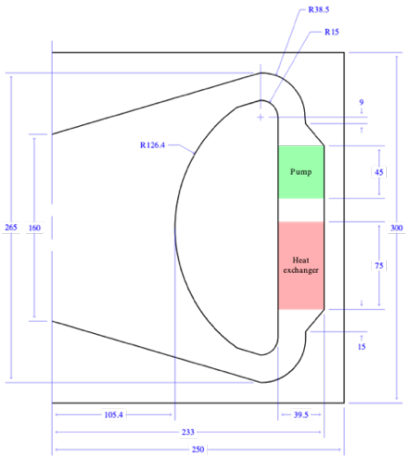

Figure 1. VTB MSFR geometry specifications.

3.2. Comparing the Results of the High-Fidelity and Calibrated Intermediate-Fidelity Model

Once the Pronghorn model is calibrated, the velocity and pressure fields obtained with Nek5000 and the calibrated Pronghorn model are compared. The 2D velocity and pressure contour plots comparison for $Re = 4 \times 10^4$ and $Re = 1 \times 10^6$ is presented in Figure 2. The Reynolds numbers are computed based on the center-height diameter and the using the average velocity across this diameter. In general, a good agreement is observed in the jet region next to the curved walls for both velocity and pressure. However, the agreement in velocity degrades towards the center part of the reactor. This is because the numerical diffusivity of Pronghorn is larger than the turbulent diffusivity away from the walls of the reactor, and thus, the turbulent model cannot be accurately calibrated in this region. This is further confirmed by analyzing the axial velocity profiles over a radial line at the mid-height in Figure 3, where Pronghorn is observed to be over diffusive towards the center of the reactor. Nonetheless, average relative L_2 errors of 6.7% and 9.9% are obtained when comparing the 2D velocity fields for $Re = 4 \times 10^4$ and $Re = 1 \times 10^6$, respectively. Similarly, average relative L_2 errors of 3.8% and 7.2% are obtained when comparing the 2D pressure fields for these Reynolds numbers. This error is acceptable for a coarse-mesh thermal-hydraulics code

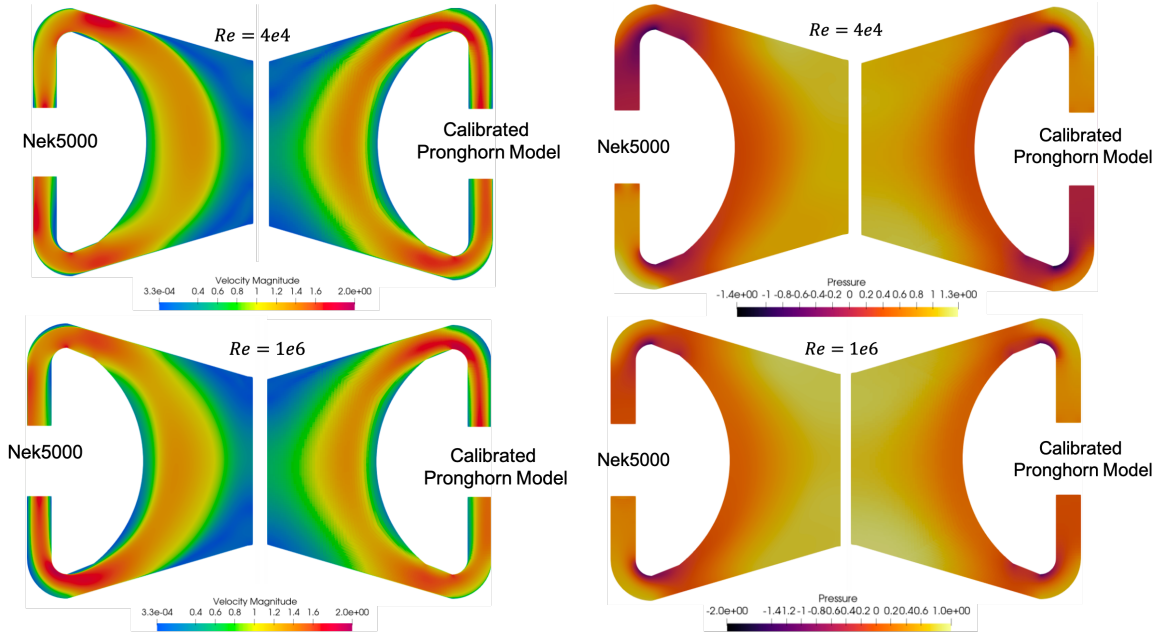

Figure 2. Comparison of the steady-state velocity (left) and pressure (right) fields for Nek5000 and the calibrated Pronghorn model for two Reynolds numbers.

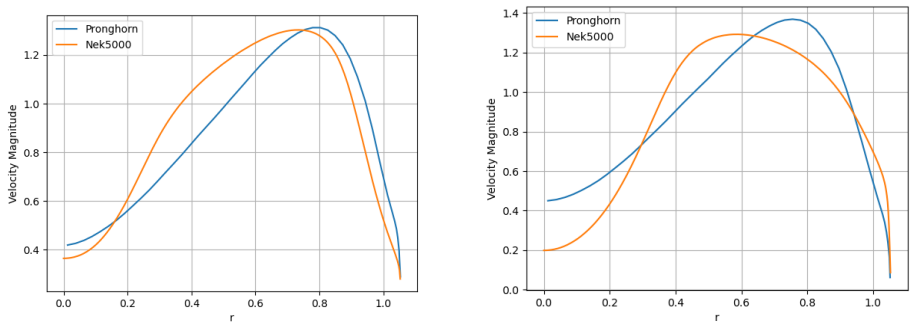

Figure 3. Comparison of the axial velocity field across the mid-height radial line between Nek5000 and Pronghorn for $Re = 4 \times 10^4$ (left) and $Re = 1 \times 10^6$ (right).

3.3. Steady-State Simulation of the Molten-Salt Fast Reactor

The calibrated Pronghorn model has been coupled to Griffin in order to perform coupled neutronics – TH simulations. We refer the reader to [2] for details about this model. Density and doppler feedbacks and delayed neutron precursors advection are considered in Griffin based on the temperature and velocity fields provided by Pronghorn. Similarly, the power source for the TH model in Pronghorn is computed using Griffin. Operation iterations are performed between both codes until a steady-state solution for the MSFR at nominal power is achieved. As an example, the velocity field and selected delayed neutron precursors families' concentration obtained are presented in Figure 4. As observed, delayed neutron precursors are advected by the flow field towards the upper part of the reactor. The velocity-induced homogenization is larger as the half-life of the delayed neutron precursor family increases towards Family 1.

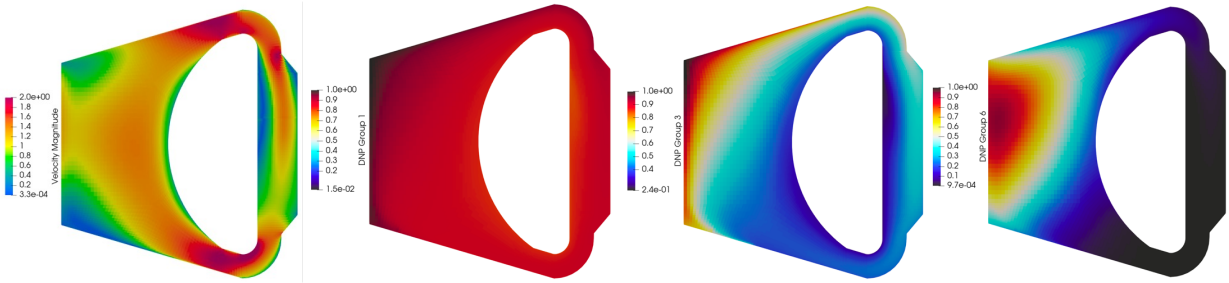

Figure 4. Left: velocity field obtained for the MSFR at nominal operation. Right: delayed neutron precursor concentration for Families 1, 3, and 6.

4. CONCLUSIONS AND FUTURE WORK

This article presents the current efforts within the VTB to improve the accuracy of the coarse-mesh thermal-hydraulics code Pronghorn by utilizing the high-fidelity thermal-hydraulics tool Nek5000. Non-intrusive and intrusive mapping methods have been described. While intrusive coupling methods involve system manipulations that require access to the numerical discretization in the models, they offer the possibility of achieving higher accuracy due to the preservation of the inherent structures of the thermal-hydraulic models during coupling. On the other hand, non-intrusive methods do not require access to the system's numerical discretization and do not necessarily preserve the physical realizability in the multi-fidelity coupling. Imposing a realizable structure in the lower fidelity tool is a way to solve this problem. We presented an example of this approach, where the capping on the mixing turbulent model in Pronghorn is calibrated via Nek5000 simulations for the MSFR, yielding L_2 errors below 10% for the velocity and pressure field predicted by the calibrated intermediate-fidelity model. The calibrated model is then coupled to the neutronics Griffin code to perform fast-running multiphysics simulations in the MSFR.

ACKNOWLEDGMENTS

This template was adapted from the template for PHYSOR 2020 posted on the Internet. Acknowledge the help of colleagues, and sources of funding, if you wish.

REFERENCES

1. "NEAMS: The Nuclear Energy Advanced Modeling and Simulation Program," ANL/NE-13/5, Argonne National Laboratory (2013).
2. A. Abou-Jaoude, S. Harper, G. Giudicelli, P. Balestra, S. Schunert, N. Martin, A. Lindsay, M. Tano, and R. Freile, "A Workflow Leveraging MOOSE Transient Multiphysics Simulations to Evaluate the Impact of Thermophysical Property Uncertainties on Molten-Salt Reactors," *Annals of Nuclear Energy*, **163**, pp. 108546 (2021). https://doi.org/10.1016/j.anucene.2021.108546.
3. P. Vegendla, R. Hu, and L. Zou, "Multi-Scale Modeling of Thermal-Fluid Phenomena Related to Loss of Forced Circulation Transient in HTGRs," ANL-19/35, Argonne National Laboratory (2019).
4. P. Balestra, S. Schunert, R. W. Carlsen, A. J. Novak, M. D. DeHart, and R. C. Martineau, "PBMR-400 Benchmark Solution of Exercise 1 and 2 using the MOOSE Based Applications: MAMMOTH, Pronghorn," *EPJ Web of Conferences*, **247** (2021). https://doi.org/10.1051/epjconf/202124706020.
5. "Overview of Advanced Reactor Simulation Capabilities to Support Demonstrations," INL/EXT-21-63162, Idaho National Laboratory (2021). https://doi.org/10.2172/1804658.
6. E. Merzari, P. Fischer, M. Min, S. Kerkemeier, A. Obabko, D. Shaver, H. Yuan, Y. Yu, J. Martinez, L. Brockmeyer, L. Fick, G. Busco, A. Yildiz, and Y. Hassan, "Toward Exascale: Overview of Large Eddy Simulations and Direct Numerical Simulations of Nuclear Reactor Flows with the Spectral Element Method in

Nek5000," *Nuclear Technology*, **206**(9), pp. 1308-1324 (2020). https://doi.org/10.1080/00295450.2020.1748557.
7. A. J. Novak, R. W. Carlsen, S. Schunert, P. Balestra, D. Reger, R. N. Slaybaugh, and R. C. Martineau, "Pronghorn: A Multidimensional Coarse Mesh Application for Advanced Reactor Thermal-Hydraulics," *Nuclear Technology*, **207**(7), pp. 1015-1046 (2021). https://doi.org/10.1080/00295450.2020.1825307.
8. Y. Wang, S. Schunert, J. Ortensi, V. Laboure, M. DeHart, Z. Prince, F. Kong, J. Harter, P. Balestra, and F. Gleicher, "Rattlesnake: A MOOSE-Based Multiphysics Multischeme Radiation Transport Application," *Nuclear Technology*, **207**(7), pp. 1047-1072 (2021). https://doi.org/10.1080/00295450.2020.1843348.
9. Y. Wang, S. Schunert, and V. Laboure, "Rattlesnake Theory Manual," INL/EXT-17-42103, Idaho National Laboratory (2018).
10. E. R. Shemon, M. A. Smith, and C. Lee, "Proteus-SN User Manual," ANL/NE-14/6 (Rev 3.0), Argonne National Laboratory (2016).
11. C. J. Permann, D. R. Gaston, D. Andrš, R. W. Carlsen, F. Konga, A. D. Lindsay, J. M. Miller, J. W. Peterson, A. E. Slaughter, R. H. Stogner, and R. C. Martineau, "MOOSE: Enabling massively parallel multiphysics simulation," *SoftwareX*, **11**, pp. 100430 (2020).
12. E. Merzari, A. Obabko, P. Fischer, N. Halford, J. Walker, A. Siegel, and Y. Yu, "Large-Scale Large Eddy Simulation of Nuclear Reactor Flows: Issues and Perspectives," *Nuclear Engineering and Design*, **312**, pp. 86-98 (2017). https://doi.org/10.1016/J.NUCENGDES.2016.09.028.
13. E. Merzari, A. Obabko, P. Fischer, and M. Aufiero, "Wall Resolved Large Eddy Simulation of Reactor Core Flows with the Spectral Element Method," *Nuclear Engineering and Design*, **364**, pp. 110657 (2020). https://doi.org/10.1016/j.nucengdes.2020.110657.
14. H. Yuan, M. A. Yildiz, E. Merzari, Y. Yu, A. Obabko, G. Botha, G. Busco, Y. A. Hassan, and D. T. Nguyen, "Spectral Element Applications in Complex Nuclear Reactor Geometries: Tet-to-Hex Meshing," *Nuclear Engineering and Design*, **357**, pp. 110422 (2020). https://doi.org/10.1016/J.NUCENGDES.2019.110422.
15. J. Fang, Y. Yu, H. Yuan, E. Merzari, and D. R. Shaver, "CFD Evaluation of Pressure Change Along Coolant Passages in Sodium-Cooled Fast Reactor with Nek5000," *Nuclear Technology* (2021). https://doi.org/10.1080/00295450.2021.1957373.
16. J. Fang, D. R. Shaver, A. Tomboulides, M. Min, P. Fischer, Y.-H. Lan, R. Rahaman, P. Romano, S. Benhamadouche, Y. A. Hassan, A. Kraus, and E. Merzari, "Feasibility of Full-Core Pin Resolved CFD Simulations of Small Modular Reactor with Momentum Sources," *Nuclear Engineering and Design*, **378**, pp. 111143 (2021). https://doi.org/10.1016/j.nucengdes.2021.111143.
17. A. Kraus, Elia Merzari, Thomas Norddine, Oana Marin, Sofiane Benhamadouche, "Direct Numerical Simulation of Fluid Flow in a 5x5 Square Rod Bundle," *International Journal of Heat and Fluid Flow*, **90**, pp. 108833 (2021). https://doi.org/10.1016/j.ijheatfluidflow.2021.108833.
18. A. Tomboulides, S. M. Aithal, P. F. Fischer, E. Merzari, A. V. Obabko, D. R. Shaver, "A Novel Numerical Treatment of the Near-Wall Regions in the k−ω Class of RANS Models," *International Journal of Heat and Fluid Flow*, **72**, pp. 186-199 (2018). https://doi.org/10.1016/J.IJHEATFLUIDFLOW.2018.05.017.
19. M. Tano, P. German, and J. Ragusa, "Evaluation of Pressure Reconstruction Techniques for Model Order Reduction in Incompressible Convective Heat Transfer," *Thermal Science and Engineering Progress*, **23**, pp. 100841 (2021). https://doi.org/10.1016/j.tsep.2021.100841.
20. J. Yu, C. Yan, and M. Guo, "Non-Intrusive Reduced-Order Modeling for Fluid Problems: A Brief Review," *Proceedings of the Institution of Mechanical Engineers, Part G: Journal of Aerospace Engineering*, **233**(16), pp. 5896-5912 (2019). https://doi.org/10.1177/0954410019890721.